

This is the Accepted Author Manuscript of the publication

**Resting-state functional MRI and [18F]-FDG PET demonstrate differences in neuronal activity between commonly used mouse strains.**

**Disha Shah<sup>a</sup>, Steven Deleye<sup>b</sup>, Marleen Verhoye<sup>a</sup>, Steven Staelens<sup>b</sup>, Annemie Van der Linden<sup>a</sup>**

<sup>a</sup> Bio-Imaging Lab, University of Antwerp, Universiteitsplein 1, 2610 Wilrijk, Antwerp Belgium

<sup>b</sup> Molecular Imaging Center Antwerp, Universiteitsplein 1, 2610 Wilrijk, Antwerp Belgium

Corresponding author:

D. Shah

[Disha.Shah@uantwerpen.be](mailto:Disha.Shah@uantwerpen.be)

Published in: Neuroimage. 2016 Jan 15;125:571-7.

Doi: 10.1016/j.neuroimage.2015.10.073

**The final publication is available at**

<http://www.sciencedirect.com/science/article/pii/S1053811915009970>

© 2015. This manuscript version is made available under the CC-BY-NC-ND 4.0 license <http://creativecommons.org/licenses/by-nc-nd/4.0/>

**Title: Resting-state functional MRI and [18F]-FDG PET demonstrate differences in neuronal activity between commonly used mouse strains.**

**Authors:**

Disha Shah<sup>1</sup>, Steven Deleye<sup>2</sup>, Marleen Verhoye<sup>1</sup>, Steven Staelens<sup>2</sup>, Annemie Van der Linden<sup>1</sup>

**Authors affiliations:**

<sup>1</sup> Bio-Imaging Lab, University of Antwerp, Universiteitsplein 1, 2610 Wilrijk, Antwerp Belgium.

<sup>2</sup> Molecular Imaging Center Antwerp, Universiteitsplein 1, 2610 Wilrijk, Antwerp Belgium

**Corresponding author:**

Disha Shah

Bio-Imaging Lab, University of Antwerp, Universiteitsplein 1, 2610 Wilrijk, Antwerp Belgium

email: [Disha.Shah@uantwerpen.be](mailto:Disha.Shah@uantwerpen.be)

Phone: + 32 (0)3 265.27.62.

## **Abstract**

The existence of numerous interesting mouse models of neurological disorders enables the investigation of causal relations between pathological events and the effect of treatment regimes. However, mouse models of a specific neurological disease are often generated using different background strains, which raises the question whether the observed effects are specific to pathology or depend on the used strain. This study used two independent in vivo functional imaging techniques to evaluate whether mouse strain differences exist in functional connectivity (FC) and brain glucose metabolism i.e. indirect measures of neuronal activity. For this purpose, C57BL/6, BALB/C and SJL mice (N=15/group, male) were evaluated using resting-state functional MRI (rsfMRI) and static [18F]-fluorodeoxyglucose Positron Emission Tomography ([18F]-FDG PET). RsfMRI and [18F]-FDG PET data were analyzed with independent component analysis (ICA). FC was quantified by calculating the mean network-specific FC strength and [18F]-FDG uptake was quantified by calculating the mean network-specific standard uptake value corrected for plasma glucose levels and body weight (SUV<sub>glu</sub>). The ICA results showed spatially similar neurological components in the rsfMRI and [18F]-FDG PET data, suggesting that patterns of metabolic covariance in the mouse brain reflect FC networks. Comparing FC and [18F]-FDG data showed that strain-dependent differences in brain activity exist for several brain networks i.e. the frontal, cingulate, (hypo)thalamus, striatum, and sensorimotor networks. The results of this study have implications for the interpretation of in vivo functional imaging data in mouse models of neurological disorders generated on different background strains.

## **1. Introduction**

Mice are the most commonly used model organism in neurological research. There is a wide plethora of transgenic mouse models of human brain disorders which allows high throughput investigations of causal relations between pathological events, disease mechanisms, the effect of treatment outcomes etc. Mouse models of neurological diseases can be generated by inducing lesions in specific brain regions, e.g. lesion models of Parkinson's disease (Iancu et al., 2005) or epilepsy (McKhann et al., 2003), or by inducing mutations in genes that are involved in specific brain disorders, such as in the amyloid-precursor protein (APP) gene for Alzheimer's disease (Hsiao et al., 1996, Radde et al., 2006). These mouse models are often created using different background strains of mice, even if these models represent a similar pathological event (Lassalle et al., 2008). This raises the question whether the background strain might interfere with observations assumed to be related or specific to a certain pathological occurrence.

There is great interest in investigating mouse models using in vivo imaging techniques, considering that their non-invasive nature allows longitudinal studies and eventually translation to the clinic. Resting-state functional MRI (rsfMRI) is a technique that is used to evaluate functional connectivity (FC) in the brain. FC is defined as the temporal correlation of low frequency fluctuations (0.01-0.1Hz) of the blood-oxygenation-level-dependent (BOLD) signal between brain regions (Biswal et al., 1995, van den Heuvel and Hulshoff Pol, 2010). The BOLD signal is an indirect measure of neuronal activity and is regionally mediated by among others brain glucose metabolism, cerebral blood flow (CBF) and cerebral blood volume (CBV). Previous studies showed that rsfMRI is able to discern several functional brain networks in healthy and transgenic mice (Shah et al., 2013). Fluorodeoxyglucose ([<sup>18</sup>F]-FDG) Positron Emission Tomography (PET) is another functional imaging technique that is used to evaluate glucose metabolism. [<sup>18</sup>F]-FDG is a glucose analog where the 2' hydroxyl group is substituted by <sup>18</sup>F. After phosphorylation [<sup>18</sup>F]-FDG cannot be further metabolized and thus gets trapped in glucose consuming cells. The cerebral uptake of [<sup>18</sup>F]-FDG relates to synaptic activity (Attwell and Laughlin, 2001). Thus, both BOLD rsfMRI and [<sup>18</sup>F]-FDG PET are valuable tools that provide indirect measures to evaluate brain activity.

This study investigates strain-dependent differences in BOLD FC and cerebral [18F]-FDG metabolism using three mouse strains i.e. C57BL/6, BALB/C and SJL mice. These strains are widely used in neurological research and as background strains to create transgenic models of human diseases. Several studies reported behavior differences between these strains regarding anxiety, spatial memory, motivated behavior and sensory functions (Crawley et al., 1997), which suggests that functional processes in the brain might also differ between these strains. The results of this study have major implications for the interpretation of functional imaging data in mouse models of neurological disorders.

## **2. Material and Methods**

### ***2.1. Ethics statement and animals***

Male C57BL/6, BALB/C and SJL mice of 12 weeks old (N=15/group) were used throughout the entire study (Jax mice strains, Charles River Laboratories). All procedures were performed in strict accordance with the European Directive 2010/63/EU on the protection of animals used for scientific purposes. The protocols were approved by the Committee on Animal Care and Use at the University of Antwerp, Belgium (permit number 2013-62) and all efforts were made to minimize animal suffering.

For the MRI handling procedures all mice were anesthetized with 2.5% isoflurane (IsoFlo, Abbott, Illinois, USA), which was administered in a mixture of 70% nitrogen (400 cc/min) and 30% oxygen (200 cc/min). During the rsfMRI imaging procedures, a combination of medetomidine (Domitor, Pfizer, Karlsruhe, Germany) and isoflurane was used to sedate the animals. After positioning of the animal in the scanner, medetomidine was administered subcutaneously as a bolus injection (0.3 mg/kg), after which the isoflurane level was immediately decreased to 1%. Five minutes before the rsfMRI acquisition, isoflurane was decreased to 0.4%. RsfMRI scans were consistently acquired 40 min after the bolus injection (Shah et al., 2015), during which the isoflurane level was kept at 0.4%. After the imaging procedures, the effects of medetomidine were counteracted by subcutaneously injecting 0.1mg/kg atipamezole (Antisedan, Pfizer, Karlsruhe, Germany). The physiological status of all animals was monitored throughout the imaging procedure. A pressure sensitive pad (MR-compatible Small Animal Monitoring and Gating system, SA Instruments, Inc.) was used to monitor breathing rate and a rectal thermistor with feedback controlled warm air circuitry (MR-compatible Small Animal Heating System, SA Instruments, Inc.) was used to maintain body temperature at  $(37.0 \pm 0.5) ^\circ\text{C}$

For the PET procedures, all mice were fasted overnight (10-13 h), after which they received an awake intravenous injection of 18.5 MBq [ $^{18}\text{F}$ ]-FDG followed by a conscious 30 min uptake time before the PET scan. Whole blood glucose levels were measured from a drop of blood from the tail vein using a blood glucose meter (One Touch Ultra 2, Lifescan, France). Anesthesia was induced by inhalation of isoflurane (5% for induction and 2% for maintenance) supplemented with oxygen. The body temperature of the animals was maintained with a heated airflow (37 °C) (Minerve, Esternay, France) and the respiration rate was monitored with a pressure pad (M2M Imaging, Cleveland, USA).

## ***2.2. Imaging procedures***

MRI procedures were performed on a 9.4T Biospec MRI system (Bruker BioSpin, Germany) with the Paravision 5.1 software ([www.bruker.com](http://www.bruker.com)). Images were acquired using a standard Bruker cross coil set-up with a quadrature volume coil and a quadrature surface coil for mice. Three orthogonal multi-slice Turbo RARE T2-weighted images were acquired to render slice-positioning uniform (repetition time 2000 ms, echo time 15 ms, 16 slices of 0.4 mm). Field maps were acquired for each animal to assess field homogeneity, followed by local shimming, which corrects for the measured inhomogeneity in a rectangular VOI within the brain. Resting-state signals were measured using a T2\*-weighted single shot EPI sequence (repetition time 2000 ms, echo time 15 ms, 16 slices of 0.4 mm, 150 repetitions). The field-of-view was (20 x 20) mm<sup>2</sup> and the matrix size (128 x 64), resulting in voxel dimensions of (0.156 x 0.312) mm<sup>2</sup>.

Static [ $^{18}\text{F}$ ]-FDG PET imaging was performed using a Siemens Inveon PET-CT scanner (Siemens Preclinical Solution, Knoxville, TN). The scanner utilizes 1.59 x 1.59 x 10 mm LSO (lutetium oxy-orthosilicate) crystals grouped in 20 x 20 blocks. The axial and transaxial field-of-views are 127 and 100 mm, respectively. The animals were scanned in a head-first-prone position. The energy and timing window were set to 350–650 keV and 3.432 ns respectively. The PET images were reconstructed using 4 iterations with 16 subsets of the 2D ordered subset expectation maximization (OSEM 2D) algorithm (Hudson and Larkin, 1994) following Fourier rebinning (FORE) (Defrise et al., 1997). Normalization, dead time, random, CT-based attenuation and single-scatter stimulation (SSS) scatter corrections (Watson, 2000) were applied. PET images were reconstructed on a 128 x 128 x 159 grid with a pixel

size of 0.776 mm and a slice thickness of 0.796 mm. Subsequent to the PET scan, CT imaging was performed using a 220 degrees rotation with 120 rotation steps. Voltage and amperage were set to 80 keV and 500  $\mu$ A, respectively.

### ***2.3. Data pre-processing***

Pre-processing of the rsfMRI data, including realignment, normalization and smoothing, was performed using SPM8 software (Statistical Parametric Mapping, <http://www.fil.ion.ucl.ac.uk>). First, all images within each session were realigned to the first image. This was done using a least-squares approach and a 6-parameter (rigid body) spatial transformation. For the network analyses of the rsfMRI data, motion parameters resulting from the realignment were included as covariates to correct for possible movement that occurred during the scanning procedure. Second, all datasets were normalized to a study specific EPI template and co-registered to an anatomical T2-weighted template (Mirrione et al., 2007). The normalization steps consisted of a global 12-parameter affine transformation followed by the estimation of the nonlinear deformations. Finally, in plane smoothing was done using a Gaussian kernel with full width at half maximum of twice the voxel size (0.31 X 0.62 mm<sup>2</sup>).

Image preprocessing of the static [18F]-FDG PET data was done in PMOD v3.3 (PMOD Technologies, Switzerland). Each individual PET image was transformed into the space of a predefined mouse brain template (Mirrione et al., 2007) by matching the individual CT images to the CT of the template and applying the same transformation to the subject's PET images. Tracer uptake values were subsequently extracted for each delineated VOI using a mouse brain VOI template predefined on the aforementioned MRI/CT template.

## **2.4. Data analysis**

### 2.4.1. Independent Component Analysis

Independent Component Analysis (ICA) was performed on the group level, i.e. all strains together, for rsfMRI and [18F]-FDG PET data using the GIFT-toolbox (Group ICA of fMRI toolbox version 2.0a: <http://icatb.sourceforge.net/>). For the rsfMRI data, which consists of space and time information, the data of each individual animal is concatenated. Then group ICA is performed using the Infomax algorithm, which was successful at generating relevant neurological components in the mouse brain in previous rsfMRI studies (Shah et al., 2013). The final step is back reconstruction of the data to single-subject independent components and time courses. For the PET data, which lacks time information, the data of all animals were concatenated before applying the Infomax algorithm. The resulting components represent inter-individual variation of [18F]-FDG uptake. ICA was performed using a pre-set of 15 components, which was shown to be appropriate to identify networks in mice (Sforazzini et al., 2013, Shah et al., 2015). All ICA components are shown as an overlay on an anatomical T2-weighted MRI template.

The comparison between rsfMRI and [18F]-FDG PET ICA components was done by calculating the percentage of spatial overlap between each [18F]-FDG PET group ICA component and rsfMRI group ICA component using the MRicron software (MRicron version 6.6, 2013, <http://www.mccauslandcenter.sc.edu/mricro/>). Spatial similarity between rsfMRI and [18F]-FDG PET ICA components was additionally determined by visual inspection.

### 2.4.2. Network analysis

For the rsfMRI and [18F]-FDG PET data, the individual regions-of-interest (ROI) that showed the highest z-scores on the ICA maps (**Figure 1**) were defined using the MRicron software (**Table 1**). These ROIs included the cingulate cortex, hippocampus, parietal association cortex, retrosplenial cortex, temporal association cortex, orbitofrontal cortex, prelimbic cortex, anterior thalamus, hypothalamus, posterior

thalamus, caudate putamen, motor cortex, auditory cortex, somatosensory cortex, visual cortex, insular cortex, piriform cortex, rhinal cortex and ventral pallidum/nucleus accumbens.

All rsfMRI data were filtered between 0.01-0.1 Hz using the REST toolbox (REST1.7, <http://resting-fmri.sourceforge.net>) and correlation coefficients between each pair of ROIs were calculated. These correlation coefficients were z-transformed using an in-house program developed in MATLAB (MATLAB R2013a, The MathWorks Inc. Natick, MA, USA) and represented in a correlation matrix. Mean z-transformed FC matrices were calculated for each group of mice i.e. C57BL/6, BALB/C and SJL mice. The individual zFC-matrices of each subject were used to calculate the mean BOLD FC strength of all brain networks identified in the ICA i.e. the average correlation of ROIs within a specific network. FC strength was then compared between strains. [18F]-FDG PET data analysis was performed using the PMOD software. The average activity concentrations (AC, in kBq/cc) for the different brain regions were extracted from the individual spatially normalized images. Next, the standard uptake value corrected for glucose levels (SUV<sub>glu</sub>) was calculated as  $SUV = AC/ID \times BW \times glu$ , where ID (kBq) is the injected dose, BW (g) is the body weight of the animal and glu (mg/dl) is the whole blood glucose level. Since [18F]-FDG was injected while the mice were awake, there could be differences in the brain uptake of [18F]-FDG between strains that are related to different muscle activity between the moment of injection and the acquisition of the scan. Therefore, ratios of network-specific SUV<sub>glu</sub> over whole brain SUV<sub>glu</sub> (i.e. SUV<sub>glu</sub> ratio) were calculated for comparison between strains. Additionally, the SUV<sub>glu</sub> ratio images were used to obtain difference maps for each strain comparison in SPM8.

#### 2.4.3. Statistical analyses

Statistical analyses of the zFC-matrices was performed using a one sample T-test in MATLAB (false discovery rate FDR correction,  $p < 0.05$ ). Statistical comparisons of the SUV<sub>glu</sub> maps in SPM8 were performed using a one way ANOVA (threshold of 10 voxels, uncorrected,  $p < 0.001$ ). Statistical comparisons of BOLD FC strength and SUV<sub>glu</sub> ratio's were performed in SPSS (<http://www-01.ibm.com/software/be/analytics/spss/>) using a one way ANOVA with Bonferroni's correction for multiple comparisons ( $p < 0.05$ ).

### **3. Results**

#### ***3.1 Independent Component Analysis***

Group ICA of C57BL/6, BALB/C and SJL mice together showed neurologically relevant networks in the rsfMRI and [18F]-FDG PET data (**Figure 1**), including the Default-Mode-like network (DMN-like) (**A**), frontal network (**B**), cingulate network (**C**), left and right sensorimotor networks (**D** and **E**), hypothalamus/thalamus network (**F**), ventral pallidum/nucleus accumbens network (**G**) and piriform network (**H**). The DMN-like network consisted of the frontal cortex, cingulate and retrosplenial cortex, hippocampus, and parts of the parietal and temporal association cortex and posterior thalamus. The frontal network consisted of the orbitofrontal, prelimbic and cingulate cortex. The cingulate network consisted of the cingulate, retrosplenial and parietal association cortex. The sensorimotor networks consisted of the auditory, visual, somatosensory, motor and temporal/parietal association cortex. The (hypo)thalamus network consisted of the hypothalamus, anterior and posterior thalamus and part of the caudate putamen. The ventral pallidum/nucleus accumbens network consisted of the ventral pallidum and nucleus accumbens. Finally, the piriform network consisted of the piriform, cingulate, insular and rhinal cortex. Interestingly, group ICA of the [18F]-FDG PET data (**Figure 1**) showed networks that were spatially similar to those identified in the rsfMRI data. **Figure S1** shows the percentage of spatial overlap between rsfMRI and [18F]-FDG ICA components. The other rsfMRI ICA components (**Figure S2**) consisted of the caudate putamen network (**I**), further subdivisions of the sensory network (**J**), cingulate network (**K**), and ventral pallidum/nucleus accumbens networks (**L** and **M**). The other [18F]-FDG PET ICA components (**Figure S3**) consisted of the left and right sensory/insular networks (**I** and **J**), the left and right anterior sensorimotor networks (**K** and **L**) and a bilateral sensory network (**M**). **Figure S4** shows the artefacts observed in the rsfMRI and [18F]-FDG ICA data.

#### ***3.2 RsfMRI BOLD functional connectivity analyses***

The mean zFC-matrices of the C57BL/6, BALB/C and SJL mice (**Figure 2A**) showed that the C57BL/6 mice demonstrate overall lower BOLD FC compared to the BALB/C and SJL mice. The graph in **Figure 2B** confirms that C57BL/6 mice consistently show a lower FC strength for all networks compared to the SJL mice. C57BL/6 mice showed a lower FC strength for all networks except the cingulate network compared to the BALB/C mice. Significant differences between BALB/C and SJL mice were observed

for the cingulate, (hypo)thalamus and striatum networks, and the frontal network showed a trend ( $p=0.08$ ). **Table 2** shows the corrected p-values for each strain comparison.

### **3.3 [18F]-FDG PET analyses**

To enable strain comparison without the interfering effect of different muscle and thus brain uptake of [18F]-FDG PET, SUVglu ratios over whole brain were assessed instead of the absolute values. SUVglu ratios were significantly different between strains (**Figure 3A**). BALB/C mice showed significantly higher SUVglu ratio's in the frontal, (hypo)thalamus and striatum networks, C57BL/6 mice showed higher SUVglu ratio's in the cingulate, sensorimotor and striatum networks, and SJL mice showed higher SUVglu ratio's in the cingulate network. **Table 2** shows the corrected p-values for each strain comparison in every network. **Figure 3B** shows difference maps of SUVglu ratios for each strain comparison ( $p<0.001$ , uncorrected) and confirms strain differences in the frontal, cingulate, sensorimotor, (hypo)thalamus and striatum regions.

### **Discussion**

The goal of this study was to investigate whether there are mouse strain differences in brain function. Functional processes in the brain were measured by two independent techniques i.e. rsfMRI and [18F]-FDG PET, which provide information on BOLD FC and brain glucose metabolism i.e. indirect measures of neuronal activity.

ICA identified several neurological networks in the rsfMRI data i.e. the DMN-like network, frontal network, cingulate network, sensorimotor networks, hypothalamus/thalamus network, ventral pallidum/nucleus accumbens network and piriform network. Interestingly, spatially similar networks were identified in the static [18F]-FDG PET data. The observation of ICA networks in static [18F]-FDG PET data suggests the presence of interregional metabolic correlations. Consistent with this notion, a recent study applied FC analyses to static [18F]-FDG PET data and observed abnormal interregional metabolic correlations in epileptic rats (Choi et al., 2014). The spatial similarity between rsfMRI and [18F]-FDG PET data observed in this study is consistent with another combined MRI/PET study which showed that similar brain networks could be identified in rsfMRI and dynamic [18F]-FDG PET data in rats (Wehrl et al., 2013). Furthermore, our results are consistent with a study in human subjects, where spatial ICA

discerned several brain networks in [18F]-FDG PET data that were comparable to those observed in rsfMRI data of the same subjects (Di and Biswal, 2012). That study concluded that regions that are functionally connected show similar inter-subject variances of glucose metabolism in the human brain. The BOLD contrast is an indirect measure of neural activity and depends on brain glucose metabolism, CBV and CBF, so each of these measures may reveal neural networks or shape BOLD FC networks. The current study demonstrated that glucose metabolism in the mouse brain shows patterns of covariance that might reflect BOLD FC. The combination of connectivity information that maps brain networks derived from rsfMRI and metabolic PET data i.e. mapping of functional and metabolic brain networks has been termed 'cometomics' (Wehrl et al., 2014).

Discrepancies in the ICA components between the rsfMRI and [18F]-FDG PET data might be explained by the fact that rsfMRI deals with BOLD data, while [18F]-FDG PET measures brain glucose metabolism. Both are indirect measures of brain function, but represent different properties hereof, which might explain similarities as well as discrepancies between rsfMRI and [18F]-FDG PET data. Another possible explanation is that in this study the rsfMRI data is dynamic, while the [18F]-FDG PET data is static. Moreover, the temporal scale for rsfMRI data is in the order of seconds, while for the [18F]-FDG PET data it is in the order of minutes. Another possible explanation is the use of anesthesia for the rsfMRI measurements, which could influence the ICA outcome to some extent. Since the research field of 'cometomics' is still in its infancies, there is still much room for further refinement of the analyses techniques and interpretation of the data.

RsfMRI demonstrated strain-dependent differences in BOLD FC in several brain networks, especially in the cingulate, (hypo)thalamus, striatum networks, and to a lesser extent in the frontal network. C57BL/6 mice demonstrated significantly lower FC for all brain networks compared to the other strains. [18F]-FDG PET showed strain differences in frontal, cingulate, sensorimotor, (hypo)thalamus and striatum networks. These networks are involved in cognitive, motor, sensory, emotional and motivational behaviour. These results demonstrate that functional processes might be different between mouse strains, which might be a reflection of the known behavioural differences between strains. Indeed, behaviour studies comparing C57BL/6, BALB/C and SJL mice demonstrate different levels of anxiety

(Owen et al., 1997, Belzung, 2001), which might involve functional differences in frontal, (hypo)thalamus and even in striatum networks, as anxiety is reflected by decreased motor movement in open field tests. BALB/C mice are known to show higher levels of anxiety compared to other strains, which is consistent with the observation of differences in BOLD FC and brain glucose metabolism in the frontal, (hypo)thalamus and striatum networks. Furthermore, differences in the (hypo)thalamus might reflect known strain differences in circadian rhythm (Schwartz and Zimmerman, 1990). Similarly, functional differences in the frontal, cingulate and striatum networks could account for behavioural differences in rewarding effects of addictive substances such as cocaine (Crawley et al., 1997, Belzung and Barreau, 2000). Functional differences in the cingulate, frontal and sensorimotor networks could reflect performance differences in spatial memory tasks such as the Morris water maze (Crawley et al., 1997, Owen et al., 1997). It has to be taken into account that although the results of this study do show some consistency with behaviour results described in the literature, it is not straightforward to link certain behavioural phenotypes to functional network changes due to the complex nature of both measures. The most important implication of the current study is that mouse strain differences exist in BOLD FC and [18F]-FDG PET data, which needs to be taken into account when interpreting data from these modalities.

When considering BOLD FC strength, C57BL/6 mice demonstrated significantly lower FC compared to the other strains. This might be an actual strain-related difference, but another possibility is that it is due to different effects of medetomidine anesthesia in the brain, which is known to affect BOLD FC (Nasrallah et al., 2014). This observation has implications for rsfMRI studies in this specific mouse strain under medetomidine anesthesia, which is used extensively for rsfMRI studies in mice. Depending on the experimental set-up, the use of other mouse strains might be more desirable. To circumvent the issues that come with the use of anesthetics, awake imaging might be an option. For the [18F]-FDG PET data acquisition, [18F]-FDG was injected when the animals were awake, so the uptake values were not influenced by anesthesia. Awake rsfMRI imaging has been performed in rats (Becerra et al., 2011, Liang et al., 2011, 2012), but in mice it is still extremely challenging, as animals still experience non-negligible stress despite acclimation training, and such conditions are not favourable when examining brain function.

To conclude, this study firstly showed that metabolic covariance patterns might reflect BOLD neural networks in the mouse brain. Secondly, strain-dependent differences exist in regional BOLD FC and

brain glucose metabolism, i.e. two indirect measures of brain activity acquired by two independent functional imaging techniques. These results suggest that specific behavioural phenotypes might be reflected as specific patterns in brain function. Finally and most importantly, this study shows that the outcome of in vivo functional imaging studies can depend on the used mouse strain, which has implications for the interpretation of functional data in mouse models of neurological disorders generated on different background strains.

**Acknowledgements:** This research was supported by the European Union's Seventh Framework Programme under grant agreement number 278850 (INMiND), by Molecular Imaging of Brain Pathophysiology (BRAINPATH) under grant agreement number 612360 within the Marie Curie Actions-Industry-Academia Partnerships and Pathways (IAPP) program, and by the Institute for the Promotion of Innovation by Science and Technology (IWT) in Flanders under grant agreement 131060. DS is holder of an IWT PhD grant. SS and SD were funded by the University of Antwerp, Belgium through an associate professor position for SS and a PhD grant for SD.

## Figures

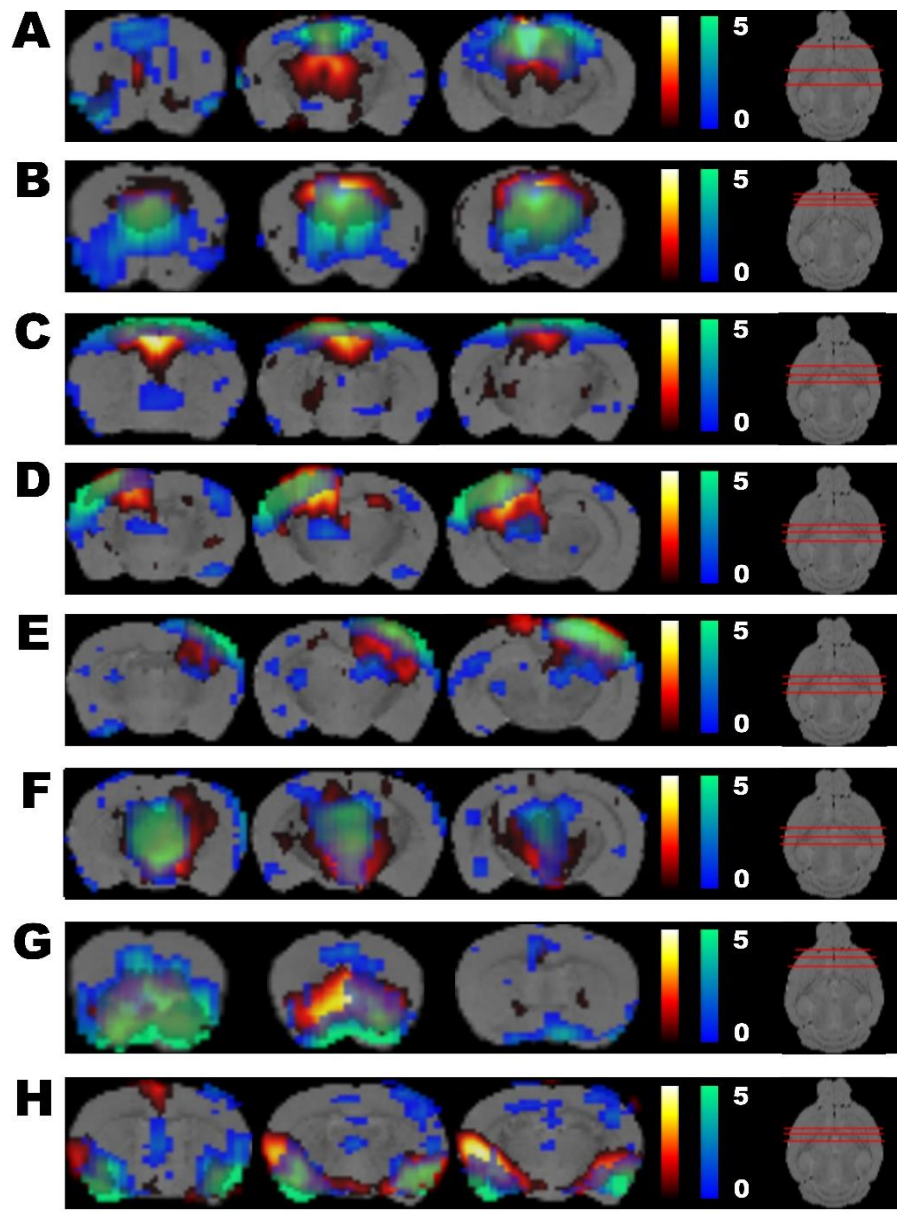


**Figure 1: Spatially similar group ICA components in the rsfMRI and [18F]-FDG PET data.** Three slices of the mean ICA components from the group ICA analysis of all strains are shown as an overlay on a T2-weighted anatomical MRI template. Mean ICA components resulting from the rsfMRI data are shown in red and mean ICA components from the [18F]-FDG PET data in green. The colour scale represents the z-score i.e. the strength of the functional correlation within each network. The position of each slice is shown on a coronal brain image. A) Default-Mode-like Network, B) frontal network, C) cingulate network, D) left sensorimotor network, E) right sensorimotor network, F) (hypo)thalamus network, G) ventral pallidum/nucleus accumbens network, H) piriform network.

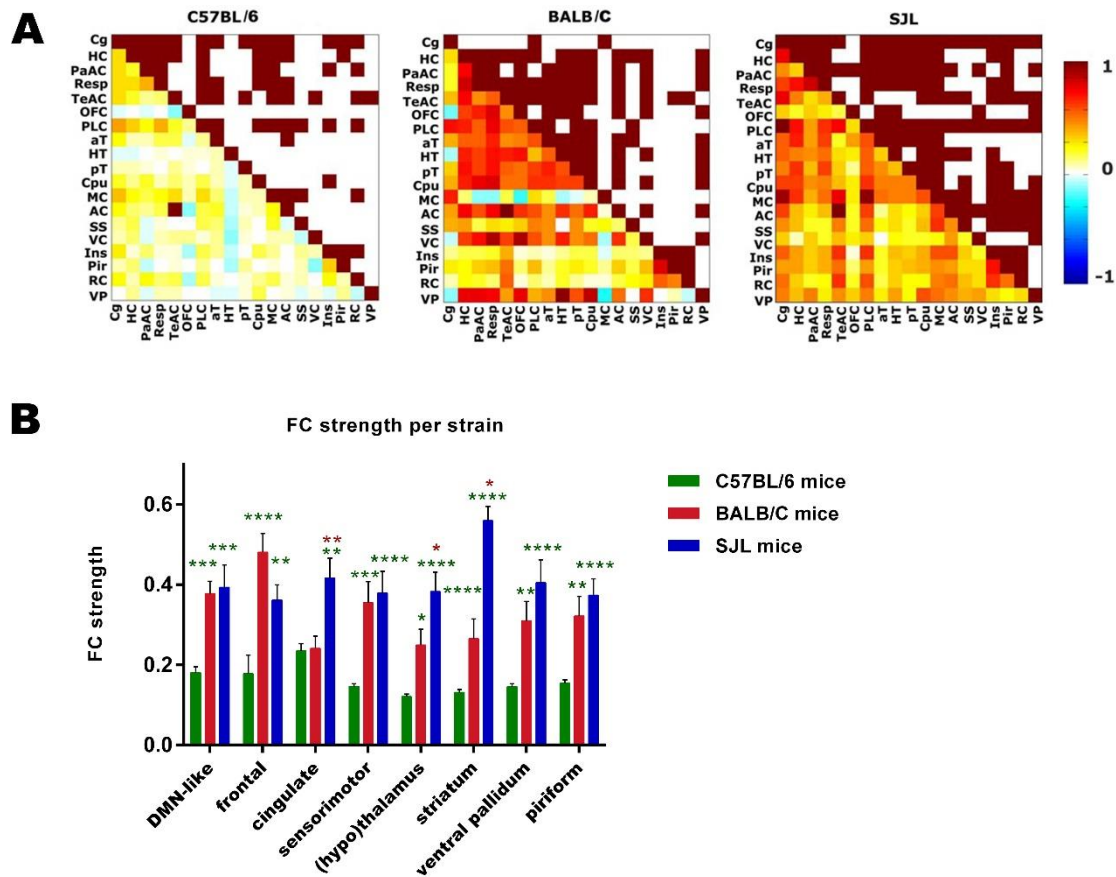


**Figure 2: BOLD functional connectivity for C57BL/6, BALB/C and SJL mice.** Panel A shows zFC-matrices of the C57BL/6, BALB/C and SJL mice. The lower half of each matrix represents the z-transformed functional correlation between each pair of brain regions, while the upper half of the matrix represents the statistically significant functional connections (red,  $p < 0.05$ , FDR-corrected). The colour scale represents the z-score i.e. the strength of the BOLD functional correlation. Abbreviations: Cg= cingulate cortex, HC= hippocampus, PaAC= parietal association cortex, Resp= retrosplenial cortex, TeAC= temporal association cortex, OFC= orbitofrontal cortex, PLC= prelimbic cortex, aT= anterior thalamus, HT= hypothalamus, pT= posterior thalamus, Cpu= caudate putamen, MC= motor cortex, AC= auditory cortex, SS= somatosensory cortex, VC= visual cortex, Ins= insular cortex, Pir= piriform cortex, RC= rhinal cortex, VP= ventral pallidum/nucleus accumbens. Panel B shows BOLD FC strength  $\pm$  standard error for each network in the C57BL/6 (green bars), BALB/C (red bars) and SJL mice (blue bars). Statistically significant differences with C57BL/6 mice are indicated by green stars, with BALB/C mice by red stars and with SJL mice by blue stars \* $p < 0.05$ , \*\* $p < 0.01$ , \*\*\* $p < 0.001$ , \*\*\*\* $p < 0.0001$ .

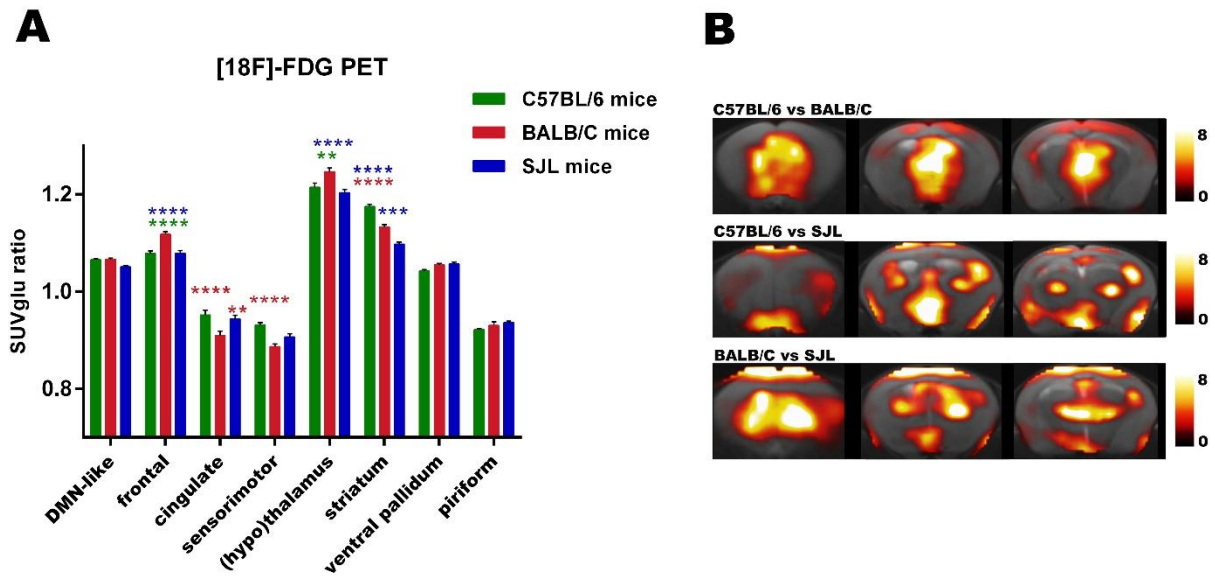


**Figure 3** Relative [18F]-FDG uptake for C57BL/6, BALB/C and SJL mice quantified as SUVglu normalized to the SUVglu of the whole brain (SUVglu ratio). **Panel A** shows the mean [18F]-FDG uptake (SUVglu ratio  $\pm$  standard error) in each brain network for C57BL/6 (green bars), BALB/C (red bars) and SJL (blue bars). Statistically significant differences with C57BL/6 mice are indicated by green stars, with BALB/C mice by red stars and with SJL mice by blue stars. \* $p < 0.05$ , \*\* $p < 0.01$ , \*\*\* $p < 0.001$ , \*\*\*\* $p < 0.0001$ . **Panel B** shows three slices of the SUVglu ratio difference maps per strain comparison. The color bar represents the F-value i.e. a measure of the SUVglu ratio difference between strains.

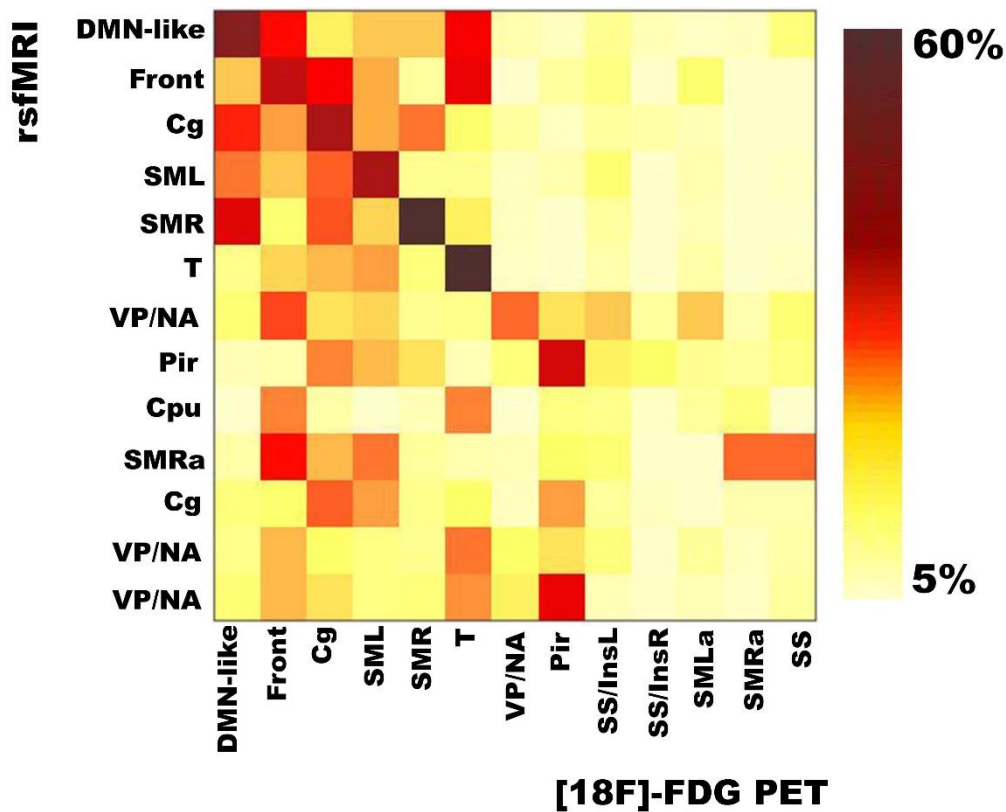


**Figure S1: Spatial overlap between rsfMRI and [18F]-FDG PET group ICA components.** Percentage spatial overlap between rsfMRI and [18F]-FDG PET group ICA components are shown in a colour coded matrix. The x-axis shows all neurological [18F]-FDG PET ICA components and the y-axis all neurological rsfMRI ICA components. Abbreviations: DMN=Default-Mode-like network, Front=frontal network, Cg=cingulate network, SML=left sensorimotor network, SMR=right sensorimotor network, T=(hypo)thalamus network, VP/NA=ventral pallidum/nucleus accumbens network, Pir=piriform network, Cpu=caudate putamen network, SMLa=left anterior sensorimotor network, SMRa= right anterior sensorimotor network, SS/InsL=left sensory/insular network, SS/InsR=right sensory/insular network, SS=somatosensory network.

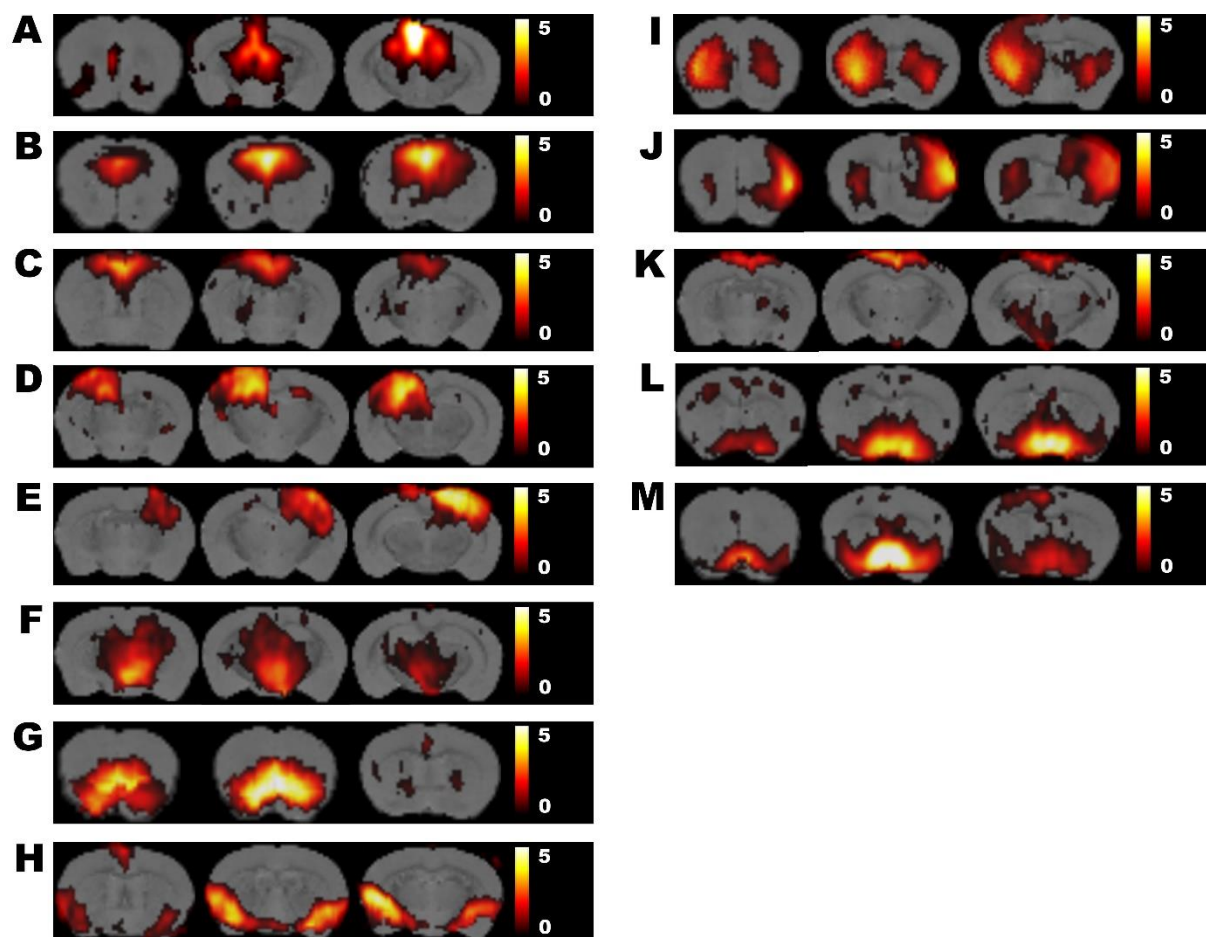


**Figure S2: Group ICA components in the rsfMRI data.** Three slices of the mean ICA components from the rsfMRI group ICA analysis of all strains are shown as an overlay on a T2-weighted anatomical MRI template. The colour scale represents the z-score i.e. the strength of the functional correlation within each network. A) Default-Mode-like Network, B) frontal network, C) cingulate network, D) left sensorimotor network, E) right sensorimotor network, F) (hypo)thalamus network, G) nucleus accumbens/ventral pallidum network, H) piriform network, I) striatum network, J) right anterior sensorimotor network, K) cingulate network, L) ventral pallidum/nucleus accumbens network, M) ventral pallidum/nucleus accumbens network

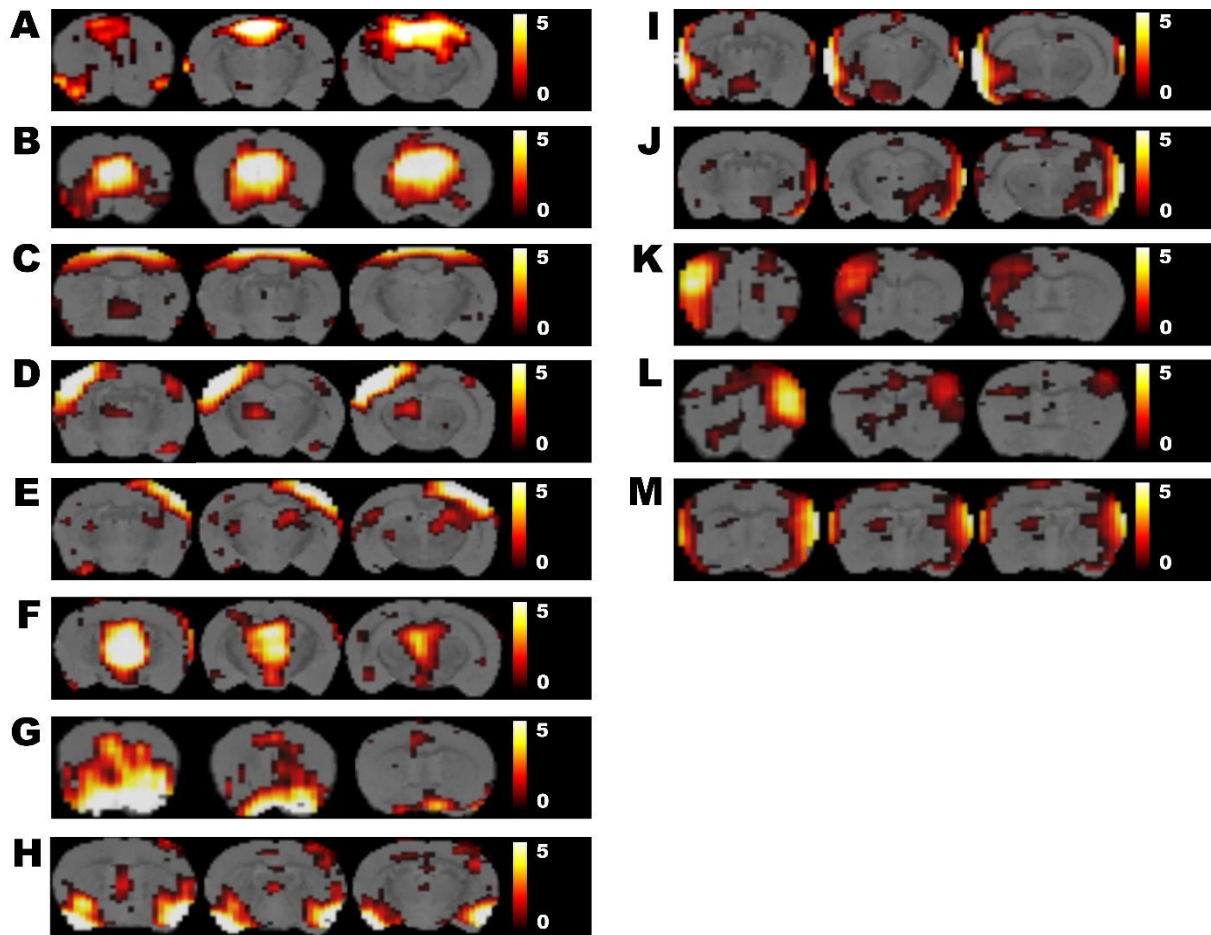


**Figure S3: Group ICA components in the [18F]-FDG PET data.** Three slices of the mean ICA components from the [18F]-FDG PET group ICA analysis of all strains are shown as an overlay on a T2-weighted anatomical MRI template. The colour scale represents the z-score i.e. the strength of the functional correlation within each network. A) Default-Mode-like Network, B) frontal network, C) cingulate network, D) left sensorimotor network, E) right sensorimotor network, F) (hypo)thalamus network, G) ventral pallidum/nucleus accumbens network, H) piriform network, I) left sensory/rhinal network, J) right sensory/rhinal network, K) left anterior sensorimotor network, L) right anterior sensorimotor network, M) sensory network.

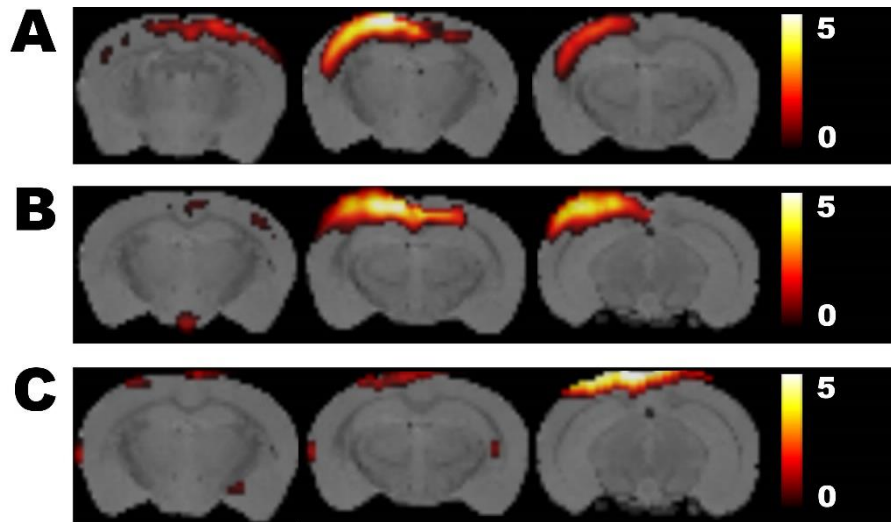


**Figure S4: Group ICA components representing artefacts in the rsfMRI and [18F]-FDG PET data.**

Three slices of the artefact ICA components resulting from the rsfMRI and [18F]-FDG PET data are shown as an overlay on a T2-weighted anatomical MRI template. The colour scale represents the z-score i.e. the strength of the functional correlation. A) RsfMRI artefact, B) RsfMRI artefact C) [18F]-FDG PET artefact.

## Reference List

- Attwell D, Laughlin SB (2001) An energy budget for signaling in the grey matter of the brain. *Journal of cerebral blood flow and metabolism : official journal of the International Society of Cerebral Blood Flow and Metabolism* 21:1133-1145.
- Becerra L, Pendse G, Chang PC, Bishop J, Borsook D (2011) Robust reproducible resting state networks in the awake rodent brain. *PloS one* 6:e25701.
- Belzung C (2001) The genetic basis of the pharmacological effects of anxiolytics: a review based on rodent models. *BehavPharmacol* 12:451-460.
- Belzung C, Barreau S (2000) Differences in drug-induced place conditioning between BALB/c and C57Bl/6 mice. *PharmacolBiochemBehav* 65:419-423.
- Biswal B, Yetkin FZ, Haughton VM, Hyde JS (1995) Functional connectivity in the motor cortex of resting human brain using echo-planar MRI. *Magnetic resonance in medicine : official journal of the Society of Magnetic Resonance in Medicine / Society of Magnetic Resonance in Medicine* 34:537-541.
- Choi H, Kim YK, Kang H, Lee H, Im HJ, Hwang do W, Kim EE, Chung JK, Lee DS (2014) Abnormal metabolic connectivity in the pilocarpine-induced epilepsy rat model: a multiscale network analysis based on persistent homology. *NeuroImage* 99:226-236.
- Crawley JN, Belknap JK, Collins A, Crabbe JC, Frankel W, Henderson N, Hitzemann RJ, Maxson SC, Miner LL, Silva AJ, Wehner JM, Wynshaw-Boris A, Paylor R (1997) Behavioral phenotypes of inbred mouse strains: implications and recommendations for molecular studies. *Psychopharmacology (Berl)* 132:107-124.
- Defrise M, Kinahan PE, Townsend DW, Michel C, Sibomana M, Newport DF (1997) Exact and approximate rebinning algorithms for 3-D PET data. *IEEE TransMedImaging* 16:145-158.
- Di X, Biswal BB (2012) Metabolic brain covariant networks as revealed by FDG-PET with reference to resting-state fMRI networks. *Brain Connect* 2:275-283.
- Hsiao K, Chapman P, Nilsen S, Eckman C, Harigaya Y, Younkin S, Yang F, Cole G (1996) Correlative memory deficits, A $\beta$  elevation, and amyloid plaques in transgenic mice. *Science* 274:99-102.
- Hudson HM, Larkin RS (1994) Accelerated image reconstruction using ordered subsets of projection data. *IEEE TransMedImaging* 13:601-609.
- Iancu R, Mohapel P, Brundin P, Paul G (2005) Behavioral characterization of a unilateral 6-OHDA-lesion model of Parkinson's disease in mice. *Behavioural brain research* 162:1-10.
- Lassalle JM, Halley H, Dumas S, Verret L, Frances B (2008) Effects of the genetic background on cognitive performances of TG2576 mice. *Behavioural brain research* 191:104-110.
- Liang Z, King J, Zhang N (2011) Uncovering intrinsic connective architecture of functional networks in awake rat brain. *The Journal of neuroscience : the official journal of the Society for Neuroscience* 31:3776-3783.
- Liang Z, King J, Zhang N (2012) Anticorrelated resting-state functional connectivity in awake rat brain. *NeuroImage* 59:1190-1199.
- McKhann GM, 2nd, Wenzel HJ, Robbins CA, Sosunov AA, Schwartzkroin PA (2003) Mouse strain differences in kainic acid sensitivity, seizure behavior, mortality, and hippocampal pathology. *Neuroscience* 122:551-561.
- Mirrione MM, Schiffer WK, Fowler JS, Alexoff DL, Dewey SL, Tsirka SE (2007) A novel approach for imaging brain-behavior relationships in mice reveals unexpected metabolic patterns during seizures in the absence of tissue plasminogen activator. *Neuroimage* 38:34-42.
- Nasrallah FA, Lew SK, Low AS, Chuang KH (2014) Neural correlate of resting-state functional connectivity under  $\alpha$ 2 adrenergic receptor agonist, medetomidine. *Neuroimage* 84:27-34.
- Owen EH, Logue SF, Rasmussen DL, Wehner JM (1997) Assessment of learning by the Morris water task and fear conditioning in inbred mouse strains and F1 hybrids: implications of genetic

- background for single gene mutations and quantitative trait loci analyses. *Neuroscience* 80:1087-1099.
- Radde R, Bolmont T, Kaeser SA, Coomaraswamy J, Lindau D, Stoltze L, Calhoun ME, Jaggi F, Wolburg H, Gengler S, Haass C, Ghetti B, Czech C, Holscher C, Mathews PM, Jucker M (2006) Abeta42-driven cerebral amyloidosis in transgenic mice reveals early and robust pathology. *EMBO reports* 7:940-946.
- Schwartz WJ, Zimmerman P (1990) Circadian timekeeping in BALB/c and C57BL/6 inbred mouse strains. *The Journal of neuroscience : the official journal of the Society for Neuroscience* 10:3685-3694.
- Sforazzini F, Schwarz AJ, Galbusera A, Bifone A, Gozzi A (2013) Distributed BOLD and CBV-weighted resting-state networks in the mouse brain. *Neuroimage*.
- Shah D, Blockx I, Keliris GA, Kara F, Jonckers E, Verhoye M, Van der Linden A (2015) Cholinergic and serotonergic modulations differentially affect large-scale functional networks in the mouse brain. *Brain structure & function*.
- Shah D, Jonckers E, Praet J, Vanhoutte G, Delgado YP, Bigot C, D'Souza DV, Verhoye M, Van der Linden A (2013) Resting state fMRI reveals diminished functional connectivity in a mouse model of amyloidosis. *PLoSOne* 8:e84241.
- van den Heuvel MP, Hulshoff Pol HE (2010) Exploring the brain network: a review on resting-state fMRI functional connectivity. *EurNeuropsychopharmacol* 20:519-534.
- Watson C (2000) New, faster, image-based scatter correction for 3D PET. *IEEE TransNuclSci* 47 (4):1587-1594.
- Wehrl HF, Hossain M, Lankes K, Liu CC, Bezrukov I, Martirosian P, Schick F, Reischl G, Pichler BJ (2013) Simultaneous PET-MRI reveals brain function in activated and resting state on metabolic, hemodynamic and multiple temporal scales. *NatMed* 19:1184-1189.
- Wehrl HF, Wiehr S, Divine MR, Gatidis S, Gullberg GT, Maier FC, Rolle AM, Schwenck J, Thaiss WM, Pichler BJ (2014) Preclinical and Translational PET/MR Imaging. *Journal of nuclear medicine : official publication, Society of Nuclear Medicine* 55:11S-18S.